Radio-frequency arbitrary waveform generation based on dispersion compensated tunable optoelectronic oscillator with ultra-wide tunability

Anle Wang (王安乐)†, Jianghai Wo (沃江海)†, Jin Zhang (张 进), Xiong Luo (罗 雄), Xin Xu (徐 馨), Daoming Zhang (张道明), Pengfei Du (杜鹏飞), and Lan Yu (余 岚)*

Microwave Photonics Center, Air Force Early Warning Academy, Wuhan 430019, China
**Corresponding author: yulann@163.com*

Received April 9, 2017; accepted July 3, 2017; posted online July 21, 2017

Photonic generation of radio-frequency (RF) arbitrary microwave waveform with ultra-wide frequency tunable range based on a dispersion compensated optoelectronic oscillator (OEO) is proposed and experimentally demonstrated. Dispersion compensation scheme and specially designed fiber Bragg grating (FBG)-based Fabry–Perot (F-P) filters are employed in the OEO loop to realize a frequency tunable range of 3.5–45.4 GHz. An optimization process provided by the combination of an erbium-doped fiber amplifier (EDFA) and FBG is employed to improve the signal-to-noise ratio (SNR) of final RF signals. The generation of linear-frequency and phase-coded microwave waveforms, with a tunable carrier frequency ranging from 4 to 45 GHz and tuned chirping bandwidths or code rates, is experimentally demonstrated.

OCIS codes: 060.0060, 350.4010, 060.5625.
doi: 10.3788/COL201715.100603.

Radio-frequency (RF) arbitrary waveform generation (AWG) has been the most common way for modern radar systems to achieve high resolution[1]. Conventional techniques to generate RF arbitrary waveforms are based on various electrical-domain techniques, which suffer the limitations of low carrier frequency, poor frequency agility, and narrow bandwidth. However, RF signals with frequency or bandwidth up to tens of GHz or higher are expected in modern radar and wireless communication systems. In addition, excellent reconfiguration and frequency agility are also urgently required. Thanks to the inherent advantages in frequency and bandwidth, microwave photonics has been suggested and investigated as an effective way to outperform electronics in term of scaling to such high frequencies[2].

So far, various techniques for photonic generation of arbitrary waveform have been proposed[3–13]. Optical pulse shaping followed by space-to-time mapping[3] or frequency-to-time mapping[4] is the most popular approach to generate arbitrary waveforms. The main underlying components in the above approach are various spatial light modulators[3] or optical spectral shapers[5], respectively. For the former, the inevitability of involving free-space optics causes the system to be lossy and makes system complicated and bulky. For the latter, once a well-designed shaper [such as a fiber Bragg grating (FBG) or its derivative products] is fixed, the generated waveform is also unchangeable, which means less reconfiguration. Another popular method is based on heterodyning two phase-correlated carriers of different frequency sweeping features[6–11]. The implementation of two phase-correlated carriers usually has two ways: two modes from a mode-locked laser[7] or two sidebands from an externally modulated light wave[8–11]. For the first case, optical filters are desired to select the needed modes. Then the selected wavelengths are separately modulated and finally beaten together at a photodetector (PD) to generate the expected arbitrary waveforms. Although, in principle, the generated signals have a carrier frequency tuning range as large as the bandwidth of the optical comb, and current optical filters, which still perform insufficiently well in bandwidth and frequency tunability, cause the frequency agility of the approach to be limited. In the second case, two sidebands can be generated directly by biasing a Mach–Zehnder modulator (MZM) at minimum transmission point or also by employing optical filters. Similarly, the frequency is also limited due to the use of optical filters. Optical multiplication techniques are developed to improve the frequency agility[12]. However, the phase noise cannot be guaranteed, especially at a high multiplication factor. What is more, an external microwave source is required in all of the second cases. To generate arbitrary waveforms with a larger frequency tunable range, an approach based on a tunable optoelectronic oscillator (OEO) was proposed by Li *et al.*[13]. In the scheme, when the OEO generates a frequency tunable microwave signal, one relative optical sideband will be generated simultaneously. A polarization modulator (PolM) is employed to apply complementary modulation to the sideband and a part of light from the OEO laser source. Then, by beating these two phase-correlated optical waves at a PD, arbitrary waveforms with carrier frequencies at 10 and 15 GHz and a maximum chirp rate of 22.5 GHz are experimentally obtained without using any external microwave source. Meanwhile, many other tunable OEOs have been proposed in recent years[14–17], which might provide lots of possibilities for waveform generation.

In this Letter, we propose and experimentally demonstrate a novel photonic RF-AWG setup capable of an ultra-wide frequency tunable range. The proposed setup is based on our specially designed OEO, the key feature of which is the introduction of a dispersion compensation scheme and a specially designed FBG-based Fabry–Perot (F-P) cavity (FBG-FP) in the OEO oscillation loop. The dispersion compensation scheme eliminates the limitation effect brought by the dispersion of a long fiber on the frequency tunable range. The FBG-FP not only provides an ultra-wide reflection bandwidth, but also an ultra-narrow transmission window in its reflection band. Moreover, a signal-to-noise ratio (SNR) optimization provided by a combination of an erbium-doped fiber amplifier (EDFA) and FBG is applied to the optical sideband before the optical–electrical conversion of the PD. The proposed technique is experimentally evaluated. Frequency-chirped and phase-coded microwave waveforms with a 4–45 GHz carrier frequency tunable range are demonstrated. For the frequency-chirped signals, a 0.01–10 GHz bandwidth range is achieved, and the maximum chirp rate is up to 50 GHz/ns. For the phase-coded signals, the temporal duration code varies from 0.1 to 100 ns, which corresponds to a code rate range of 0.01–10 Gb/s.

The schematic diagram of the proposed waveform generation system based on dispersion compensated OEO (DCOEO) is shown in Fig. 1. A light wave generated by a tunable laser source (TLS) is sent to an optical coupler (OC1) via a polarization controller (PC1). Then, the light is divided into two parts: one is sent to the DCOEO through a phase modulator (PM1), while the other part is sent to PM2. The DCOEO mainly consists of a PM (PM1), a homemade FBG-FP, which acts as an optical filter, two single-model fibers (SMF1, SMF2), relative dispersion compensation fibers (DCF1, DCF2), two PDs (PD1, PD2), and two electrical amplifiers (LNA1, PA1). Two features of the DCOEO are worth mentioning: firstly, dual loops are adapted for mode selection; secondly and creatively, in order to eliminate the limitation effect on the frequency tunable range of the OEO caused by the dispersion of a long SMF, the dispersion compensation scheme is used in each loop. The homemade filter consists of an optical circulator and an FBG-FP. PM1 and the optical filter together compose a tunable microwave photonic filter and complete the phase-modulation to intensity-modulation conversion. The frequency of the generated microwave waveform can be tuned by changing the wavelength of the laser.

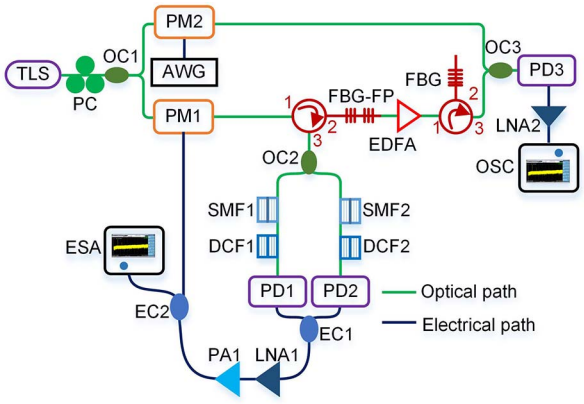

Fig. 1. Schematic diagram of the proposed AWG system based on DCOEO.

When the OEO oscillates, the FBG-FP reflects the first-order sidebands (say the upper) to the OEO loop and lets one of the left lower sidebands pass. Then, the lower sideband is amplified by an EDFA and filtered by a FBG whose reflection band covers the notch of the FBG-FP. The combination of an EDFA and FBG is used to enhance the light intensity of the lower sideband and eliminate the spontaneous emission noise of EDFA, that is, it improves the ultimate SNR of the microwave waveform. Then, the light wave is combined with the optical wave from PM1. With an electrical AWG, different modulations, such as frequency-chirped or phased-code information, can be applied to the optical wave through PM1. By beating the two light waves at another PD (PD3), an arbitrary microwave waveform is generated.

Experiments, as schematically illustrated in Fig. 1, are performed to demonstrate the AWG capability. A wavelength-tunable laser diode (ID photonics, DX4) is applied to generate continuous light waves. The optical carrier is sent to two PMs (PHOTLINE, MPZ-LN-40) to be modulated in phase. The FBG-FP has a notch located at 1550.32 nm, and its reflection bandwidth is 2.722 nm, which corresponds to 340 GHz, which in principle determines the frequency tunable range of the OEO to be over 80 GHz without any limitations. The length of two SMFs in OEO loops is 600 and 4000 m, respectively. Relatively, two DCFs used for dispersion compensation are 90 and 340 m long, corresponding to total dispersion indices of 12.6 and 47.6 ps/nm at 1550 nm, respectively. Light waves from two DCFs are sent to PD1 and PD2, separately (Finisar, HPDV2120R), to be converted into electrical signals. A low noise amplifier (KEYSIGHT, N4985-90001N) with a 32 dB gain and a power amplifier (SHF, 807) with a 29 dB gain are followed to amplify the electrical signal. Then, the amplified electrical signal is sent to PM1 to close the DCOEO loop. As we know, employing a long fiber is the common way to reduce the phase noise of the OEO. However, the dispersion of the fiber will change the frequency transmission property of the OEO loop in here, which will limit the OEO's frequency tunable range. Thus, relative DCFs are added into each loop to eliminate the limitation. An experiment for eliminating the limitation effect is carried out. The TLS wavelength is tuned at 1550.04 nm, and the expected oscillation frequency is about 35 GHz. Figure 2(a) shows the open-loop frequency spectra response of the OEO, measured by a vector network analyzer (VNA, KEYSIGHT, N5244A), before (red line) and after (yellow line) adding DCFs. It can be seen clearly that when there is no DCF, the peak (corresponding to the expected oscillation frequency) of the red line is at the 24.4 GHz, while an obvious peak

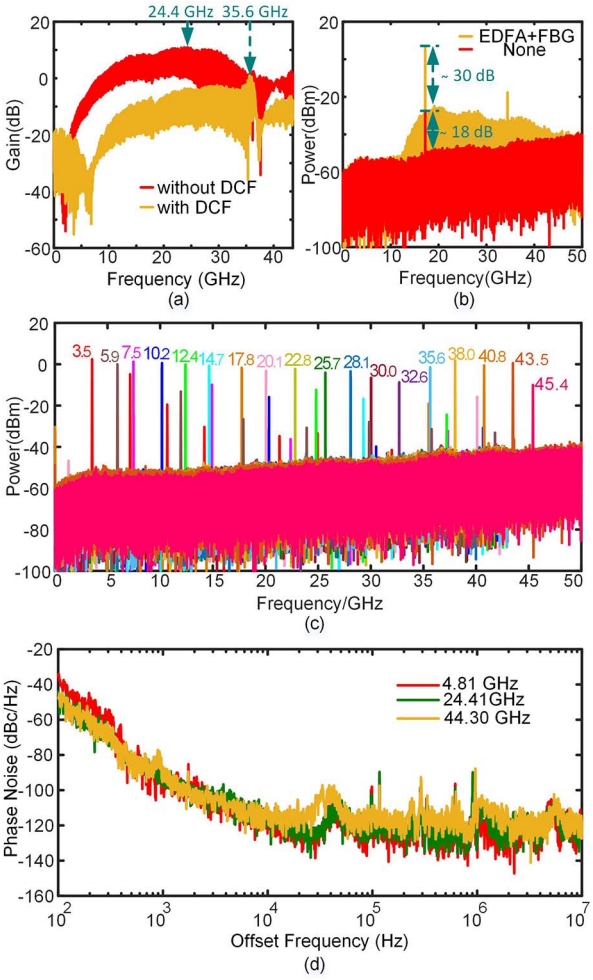

Fig. 2. (Color online) (a) Effect of dispersion compensation on broadening the frequency tunable range of the OEO. (b) Effect of the combination of an EDFA and FBG on the SNR of the frequency-beaten signal. (c) Spectra of the generated microwave signal at different frequencies. The frequency is tuned from 3 to 45 GHz. (d) SSB phase noise of the oscillation frequencies at 4.81, 24.41, and 44.30 GHz, which are generated by the DCOEO.

in the yellow line locates at the expected 35 GHz. Thus, the existence of DCFs does make the expected oscillation frequency appear. According to this, by adjusting the laser wavelength continuously from 1550.29 to 1549.96 nm, the oscillation signal with the frequency range from 3 to 45 GHz can be observed, as shown in Fig. 2(c). Based on this, the final limitation factor of the tunable frequency range is the performance of hardware used in the DCOEO loop. Furthermore, as shown in Fig. 2(d), the phase noise performance of the DCOEO is measured by a signal analyzer (KEYSIGHT, N9040B, 3–50 GHz). The single sideband (SSB) phase noises of the generated 4.81, 24.41, and 44.30 GHz signals by the proposed OEO are −120.77, −114.16, and −112.93 dBc/Hz, respectively, at an offset of 10 kHz.

When the OEO starts oscillating, an optical sideband outputs at the other end of the FBG-FP. This signal is usually very weak (∼ − 27 dBm in the experiment). Thus, an EDFA is adapted to amplify the weak sideband, and an FBG is used to filter out the spontaneous emission noise of the EDFA. Then, the expected arbitrary waveform or single-frequency RF signal is obtained by beating the filtered optical sideband with the light wave from PM2 at PD3, depending on whether PM2 is driven or not. Figure 2(b) shows the enhancement effect, brought by the combination of an EDFA and FBG, on the SNR of the generated electrical signal. Lines with different colors correspond to different situations: yellow line represents employing the combination to improve the SNR, while the red line represents the directly beating situation. Clearly, optical amplification and filtering enhance, not only, the final electrical RF power, but also its SNR (from 18 to 30 dB).

Based on the SNR optimization above, when the driving signal of PM2 generated from an AWG (KEYSIGHT, M8195A) is a frequency-chirping signal or a phase-coding signal, PD2 will generate relative frequency-chirped or phase-coded signals. Parameters of the generated signals can be adjusted by programming the driving signal. A digital storage oscilloscope (KEYSIGHT 93204A) is employed to monitor and record the temporal waveform of the generated signals. A signal filtering algorithm and the Hilbert-transform algorithm are adapted to extract the instantaneous frequency information or phase information from the recorded waveforms.

In the experiment, the DCOEO is first tuned to generate a 27 GHz microwave carrier. The half-wave voltage of the PM is 7 V. With a parabolic driven signal whose peak-to-peak voltage is 5 V, and the time duration is 85 ns; the expected bandwidth of the generated frequency-chirped signal is about 10 MHz. Figures 3(a) and 3(b) show the experimental results of the temporal waveform and the relative instantaneous frequency information recovered from the recorded waveform data. Clearly, the frequency increases almost lineally from 27.524 to 27.535 GHz, which is close to the calculated value. Similarly, as the driving signal changes into a 13 bit Baker code sequence of 10 Mb/s, a relative phase-coding waveform is generated. Figures 3(c) and 3(d) show the recorded phase-coding experimental results of the waveform and the phase information recovered from Fig. 3(c). As can be seen, the recovered phase agrees well with the 13 bit Baker code pattern, and the phase shift is about 3.18 rad, which is also close to the expected value.

In order to show the bandwidth reconfiguration capability, microwave waveforms with different bandwidths or phase-coding rates are also generated. By adjusting the time duration of the parabolic driven signal to 0.285 ns and the rate of phase-coding signal to 10 Gb/s, microwave waveforms with a 10 GHz bandwidth and a 10 Gb/s coded phase can be generated. Figure 4 shows the recorded experimental waveforms with reconfigured parameters. Figures 4(a) and 4(b) are the frequency-chirping waveform and its recovered instantaneous frequency information. As can be seen, the instantaneous frequency chirps from 32.1 to 22.0 GHz, which corresponds to a chirp rate

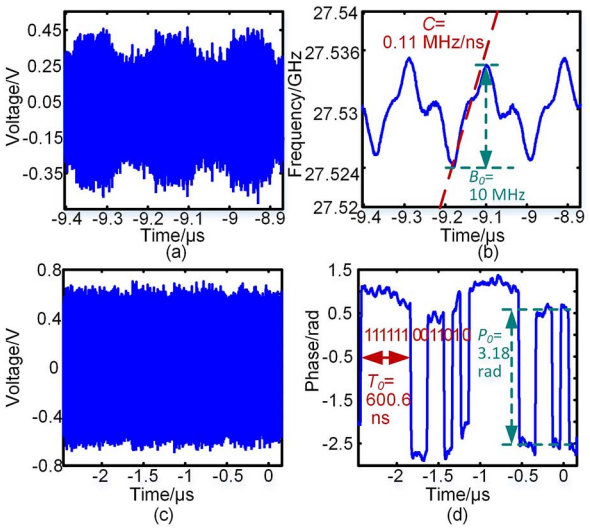

Fig. 3. (a) Generated temporal waveform and (b) the recovered instantaneous frequency profile of the linearly frequency-chirped 27 GHz signal with 10 MHz bandwidth, and (c) the waveform and (d) the recovered phase profile of the 10 Mb/s phase-coded 27 GHz signal.

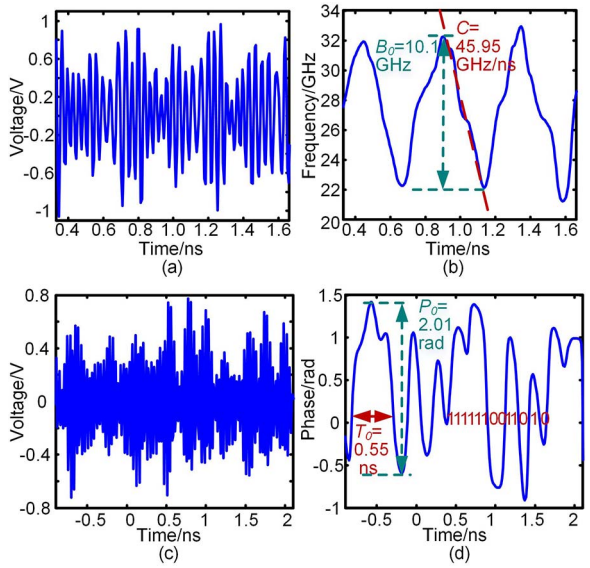

Fig. 4. (a) Generated temporal waveform and (b) the recovered instantaneous frequency profile of the linearly frequency-chirped 27 GHz signal with 10 GHz bandwidth, and (c) the waveform and (d) the recovered phase profile of the 10 Gb/s phase-coded 27 GHz signal.

of about 49.95 GHz/ns. Figures 4(c) and 4(d) are the experimental results corresponding to the 10 Gb/s phase-coding driving signal. As can be seen from Fig. 4(d), the recovered phase change agrees with the 13 bit Baker code pattern, and the time duration of the first six codes is 0.55 ns. Compared to Fig. 3(d), the quality of the recovered phase profile decreases, as demonstrated by the time duration of code and the phase shift value (2.01 rad). That may be caused by the performance decrease of the PM and PD when the bandwidth is large. Pulse compression ratios (PCRs) of the 27 GHz phase-coded microwave signals are calculated by autocorrelation processing, which are shown in Fig. 5. Figure 5(a) shows the results for the 10 Mb/s phase-coded 27 GHz signal, corresponding to Fig. 3(c). Figure 5(b) shows the results for the 10 Gb/s phase-coded 27 GHz signal, corresponding to Fig. 4(c). The peak-to-sidelobe ratios (PSRs) are 8.33 and 3.34, and the PCRs are 12.9 and 7.2, respectively.

Frequency agility is another important ability for modern radar systems, especially when radar suffers adverse atmosphere or mutual interference from a rival or friendly source. In the proposed approach, microwave carrier frequency can also be changed easily and quickly by tuning the wavelength of the laser source. To demonstrate the frequency agility of the proposed system, waveform generation experiments are carried out with carrier changed from 4 to 45 GHz. In the experiments, the frequency-chirping bandwidth is designed to be 2 GHz, and the phase-coding rate is designed to be 2 Gb/s. These driving signals are chosen by considering the parameter limitations of elements adopted in the system. Figure 6 is the experimental results with the 4 GHz carrier. Figures 6(a) and 6(c) are the measured temporal waveforms corresponding to the frequency-chirped signal and the phase-coding signal, respectively. Figures 6(b) and 6(d) are the recovered instantaneous frequency information and phase information using the Hilbert transform, respectively. The carrier frequency is exactly 4.8 GHz. The recovered results have a better linearity [Fig. 6(b)] compared with Figs. 3(b) and 4(b) and a medium-level phase-code pattern [Fig. 6(d)] compared with Figs. 3(d) and 4(d). Figure 7 shows the 45 GHz experimental results. Figures 7(a) and 7(c) are the measured temporal waveforms corresponding to the frequency-chirped signal and the phase-coding signal, respectively. Figures 7(b) and 7(d) are the recovered instantaneous frequency information and phase information using the Hilbert transform, respectively. As seen clearly in Fig. 7(b), the maximum instantaneous frequency can reach up to 45.8 GHz. Since the 3 dB bandwidth of the PMs is limited, the realized maximum bandwidth is only 1.6 GHz. For the same

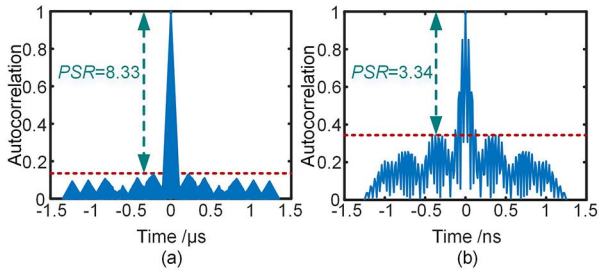

Fig. 5. Calculated autocorrelation of the phase-coded microwave waveforms with a carrier frequency of 27 GHz, and a Baker phase-coding signal with a length of 13 bit at (a) 10 Mb/s and (b) 10 Gb/s.

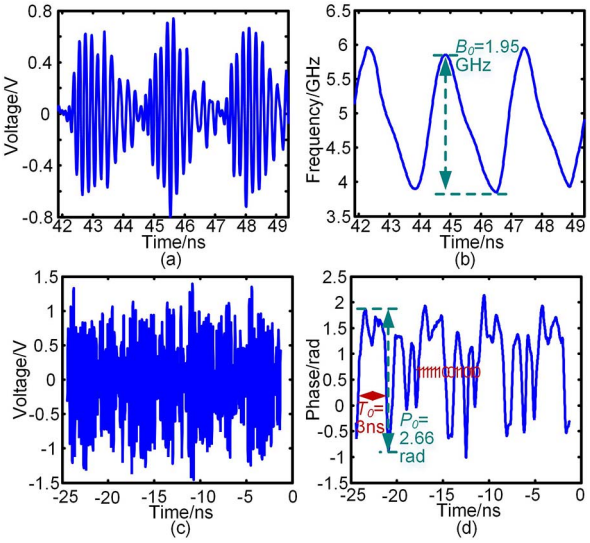

Fig. 6. (a) Generated temporal waveform and (b) the recovered instantaneous frequency profile of the linearly frequency-chirped 4 GHz signal with 2 GHz bandwidth, and (c) the waveform and (d) the recovered phase profile of the 2 Gb/s phase-coded 27 GHz signal.

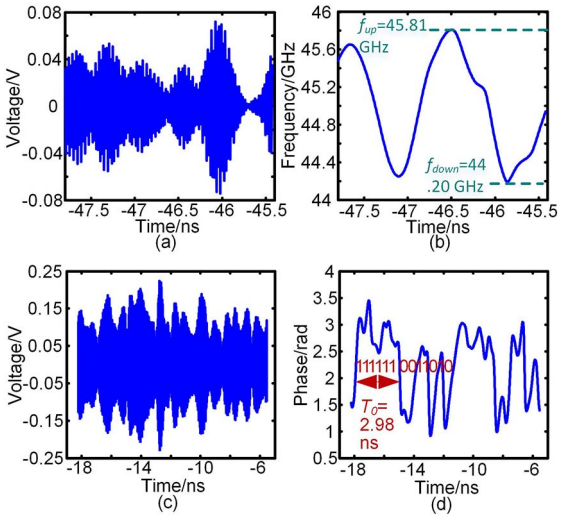

Fig. 7. (a) Generated temporal waveform and (b) the recovered instantaneous frequency profile of the linearly frequency-chirped 45 GHz signal with 2 GHz bandwidth, and (c) the waveform and (d) the recovered phase profile of the 2 Gb/s phase-coded 45 GHz signal.

reason, the recovered phase-coding signal in Fig. 7(d) has a much smaller phase shift compared to the expected π rad. The PCR of the 45 GHz phase-coded microwave signals is also calculated in the same way. The PSR and the PCR are 2.77 and 8.64, respectively. As can be seen from Figs. 5(a) and 5(b), the PSR decreases as the frequency and bandwidth increases, which can be improved by increasing the modulation voltage or changing to a better PM. However, it can still be seen that the phase-code pattern agrees with the 13 bit Baker code from Fig. 7(d).

The generated waveforms above show the excellent reconfiguration capability and frequency agility of the proposed system. The former is important for various applications, such as remote sensing and radar. The latter means potential applications in the frequency-agile radar systems and wireless communication systems. For applications in radar, our 4–45 GHz frequency tunable range covers five radar bands (C, X, Ku, K, and Ka), which again shows the distinct advantage of photonic generation of a microwave signal. However, from the application point of view, the quality of the generated waveforms need to be improved, such as the SNR of waveforms, the accuracy of phase shift, and the utility of amplitude-frequency characteristics.

In conclusion, we propose and experimentally demonstrate an RF-AWG system based on DCOEO. Thanks to the dispersion compensation adopted in the OEO loop and the SNR optimization brought by the combination of an EDFA and FBG, frequency-chirped and phase-coded waveforms can be produced with excellent reconfiguration ability, such as 4–45 GHz frequency agility, ultra-wide tunable bandwidth, or temporal duration. In the future, the enhancement of waveform quality will be the research focus.

†The authors contributed equally to this work.

References

1. D. Barton, IEEE Aerosp. Electron. Syst. Mag. **20**, 23 (2005).
2. P. Ghelfi, F. Laghezza, F. Scotti, G. Serafino, A. Capria, S. Pinna, D. Onori, C. Porzi, M. Scaffardi, and A. Malacarne, Nature **507**, 341 (2014).
3. J. D. Mckinney, D. E. Leaird, and A. M. Weiner, Opt. Lett. **27**, 1345 (2002).
4. C. Wang and J. Yao, IEEE Photon. Technol. Lett. **24**, 1493 (2012).
5. C. Wang and J. Yao, IEEE Photon. Technol. Lett. **21**, 1375 (2009).
6. Z. Li, W. Li, H. Chi, X. Zhang, and J. Yao, IEEE Photon. Technol. Lett. **23**, 712 (2011).
7. P. Ghelfi, F. Scotti, F. Laghezza, and A. Bogoni, J. Lightwave Technol. **30**, 1638 (2012).
8. Y. Zhang and S. Pan, Opt. Lett. **38**, 766 (2013).
9. X. Li, S. Zhao, Z. Zhu, K. Qu, T. Lin, and S. Pan, Chin. Opt. Lett. **15**, 070603 (2017).
10. H. Chen, T. Ning, J. Li, L. Pei, J. Yuan, and X. Wen, Chin. Opt. Lett. **15**, 060605 (2017).
11. S. Liu, Z. Qian, R. Wang, T. Pu, and T. Fang, Chin. Opt. Lett. **10**, 120401 (2012).
12. X. Li, S. Zhao, Y. Zhang, Z. Zhu, and S. Pan, IEEE Photon. Technol. Lett. **28**, 1980 (2016).
13. W. Li, F. Kong, and J. Yao, J. Lightwave Technol. **31**, 3780 (2013).
14. B. Yang, X. Jin, Y. Chen, J. Zhou, X. Zhang, S. Zheng, and H. Chi, IEEE Photon. Technol. Lett. **25**, 921 (2013).
15. Z. Z. Tang, S. L. Pan, D. Zhu, R. H. Guo, Y. J. Zhao, M. H. Pan, and D. Ben, and J. P. Yao, IEEE Photon. Technol. Lett. **24**, 1487 (2012).
16. Y. Wang, X. Jin, Y. Zhu, X. Zhang, and S. Zheng, and H. Chi, IEEE Photon. Technol. Lett. **27**, 947 (2015).
17. J. Dai, Y. Dai, F. Yin, Y. Zhou, J. Li, Y. Fan, and K. Xu, Chin. Opt. Lett. **14**, 110701 (2016).